

Thick DyBCO/YBCO Multilayer Films on LaMnO₃ Substrate Derived by Metal Organic Deposition Method

Chuan-wei Cui^{1,2} · Zhi-yong Liu^{1,2} · Jian-xin Lin¹ · Yan-qun Guo^{1,2} · Feng Fan^{1,2} · Chuan-bing Cai^{1,2}

Received: 8 January 2016 / Accepted: 20 January 2016 / Published online: 15 February 2016
© Springer Science+Business Media New York 2016

Abstract DyBa₂Cu₃O_{7-δ}/YBa₂Cu₃O_{7-δ} multilayer thick films were prepared on oxide-buffered Hastelloy substrates by low fluorine metal organic deposition (MOD) process with a thickness ranging from 0.7 μm to 2.8 μm. In the thickness of 1.4 μm sample, transition temperature (T_c) and critical current density (J_c) are 91.2 K and 2.5 MA/cm² (at 77 K, self field) respectively. With increasing thickness, T_c drops as well as J_c . Unfortunately, the critical current (I_c) does not reach an ideal value when the thickness is 2.8 μm just only 365A/cm width as thickness is 2.1 μm. Rough surface structure, compressive, and tensile stress in the interlamination and Ba-Cu-O mixed phase were found in layer thickness of 2.1 μm and 2.8 μm are assumed to be the main reason for the limitation of the current transport.

Keywords Coated conductors · DyBCO/YBCO multilayer · MOD · Thick film

1 Introduction

Second-generation high-temperature superconducting wires based on the REBa₂Cu₃O_{7-δ} (REBCO, Re = Y, Gd, Sm, Dy, etc.)-coated conductors (CCs) have emerged as hot topics due to power transport and device applications in high

magnetic fields [1–3]. Among various approaches making superconducting layer, the metal organic deposition (MOD) is an attractive technique for low-cost, high-rate deposition of REBCO CCs, applicable in atmosphere ambient pressure, in comparison with other methods including PLD [4–11].

For the commercialization of CCs, there exist two critical issues, i.e., the achievement of high production rate and the improvement of J_c properties. Therefore, major efforts are made to optimize deposition processes, conductor architecture, and material properties [12]. It is reported that critical current density (J_c) values and flux pinning force density can be improved by adding elements to YBCO samples [4, 5]. In particular, it is worthwhile to notice that RE doping can result in a significant enhancement of J_c for REBCO superconductors [13, 14]. In MOD process, RE doping can be easily realized, as the composition of the films can be easily changed through chemical modification in the MOD precursor solution.

In our previous work, it is observed that understanding the dependence is important, as the thickness of the superconducting layer is one way to enhance the transport current of coated conductors. We focus on the limitation of I_c due to structural changes with increasing YBCO thickness for the case of the IBAD-MgO metallic substrate buffered by LaMnO₃ (LMO).

By studying the crystalline orientation, morphology and surface quality, and critical current density, we attempt to understand the main reason for the limitation of the current transport on DyBCO/YBCO in low fluorine MOD process.

2 Experimental

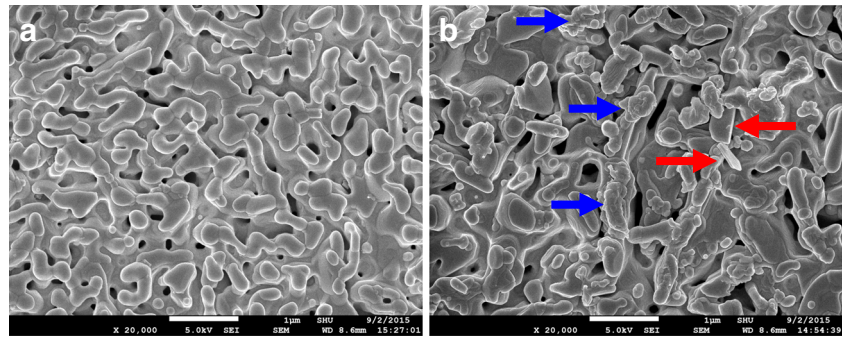
Stoichiometric quantities of Y, Dy, and Ba acetates were dissolved in de-ionized water with an excess stoichiometric

✉ Chuan-bing Cai
cbcai@shu.edu.cn

¹ Shanghai Key Laboratory of High Temperature Superconductors, Physics Department, Shanghai University, Shanghai 200444, China

² Shanghai Creative Superconductor Technologies Co. Ltd., Shanghai, 201400, China

Fig. 1 SEM images of **a** 1.4 μm and 2.8 μm -thick films showing the typical granular structure of DyBCO/YBCO. **b** Elongated *a*-axis grain are marked with red arrows and Ba-Cu-O impure phase are marked with blue arrows



quantity of trifluoroacetic acid, Cu (Dy: Ba: Cu = 1: 2: 3.3; Y: Ba: Cu = 1: 2: 3.3) acetate was dissolved in de-ionized water with an excess of propionic acid to get the coating solution. The next step in solution preparation was refining the solution by drying, and redissolving in methanol several times. This process removed the excess acetic acid, water, and other impurities from the solution. Finally, the Y/Dy, Ba, and Cu solutions were mixed, evaporated, and diluted in propionic acid to control the viscosity substrates by dip-coating.

Next, Y/DyBCO precursor films are deposited on Hastelloy/ $\text{Al}_2\text{O}_3/\text{Y}_2\text{O}_3/\text{IBAD-MgO}/\text{LaMnO}_3$ substrate by a coating process and various thicknesses are obtained by changing the coating times. For a certain sample, each coating process is kept the same. The concentration of the used precursor solution is 2.5 mol/L. Subsequently, continuous heated treatment is applied including three steps: (1) low-temperature paralysis; (2) high-temperature crystallization, and (3) annealing oxygenization. The consuming time for obtaining such as four times coated YBCO thick film is about 5 h, which is reduced greatly compared with other reports [15].

X-ray diffraction θ - 2θ scans and φ -scans (Philips X' Pert PRO, Cu Ka, $\lambda = 1.54185 \text{ \AA}$) are measured to evaluate the structure and the texture of the grown films. In order to get the quantitative estimate of the *a*-axis/*c*-axis volume fraction, we adopted the following procedure. After a χ rotation of about 57° , the (102) reflection intensity is optimized with respect to ω and 2θ . Then, a χ -scan in the range 15° to 70° is performed. The (102) planes of (100)- and (001)-oriented grains show a different tilt angle χ . Therefore, the reflections due to *a*-axis grains and to *c*-axis grains are completely separated. Raman spectroscopy (INVIA) is used to investigate residual stress in the film. The surface and cross-section image is observed with an scanning electron microscope (Ap0110300). The critical current density (J_c) of the YBCO-coated conductor is examined by inductive measurement using a Cryoscan by Theva, and the voltage criteria for J_c measurement is 50 μV .

3 Results and Discussion

3.1 Surface Morphology and Texture Analysis

A top view SEM image of 1.4 μm and 2.8 μm -thick films are shown in Fig. 1. The typical structure of DyBCO/YBCO with merging islands and pinholes are found for 0.7 μm and 1.4 μm -thick films (Fig. 1a). The island becomes larger and more separated from each other with increasing film thickness. The typical grain size increase from 0.3 μm ($d = 1.4 \mu\text{m}$) to 0.8 μm ($d = 2.8 \mu\text{m}$). This is also reflected in the width of YBCO(OOI) peak in the θ - 2θ scans, where the peaks get narrower with increasing thickness (data is not shown). Elongated *a*-axis (marked with red arrows in Fig. 1b) and Ba-Cu-O impure phase (marked with blue arrows in Fig. 1b) are visible above 0.7 μm .

The separation and enlargement of the grains is also evident in the RMS values and the average height of the surface top-view graph obtained by AFM in $5 \times 5 \mu\text{m}^2$ and $10 \times 10 \mu\text{m}^2$ scans (Table 1 and Fig. 2). The RMS value rises from about 20 nm ($d = 0.7 \mu\text{m}$) to 40 nm ($d = 2.1 \mu\text{m}$). A further distinct increase with thickness to a value of 70 nm ($d = 2.8 \mu\text{m}$) is only visible at the 10- μm scale, due to the emerging disoriented grains. The same applies for the average height, providing more realistic values of the extension of vertical structures on the surface. On the local 5- μm scale, the RMS and average height values are comparable to the values measured at thinner films. We did not observe indications of cracks or delamination, even in 2.8- μm -thick films.

Table 1 RMS values to be RMS values for various thick films

d (μm)	RMS (nm)	
	5 μm	10 μm
0.7	21	24
1.4	27	30
2.1	38	43
2.8	58	67

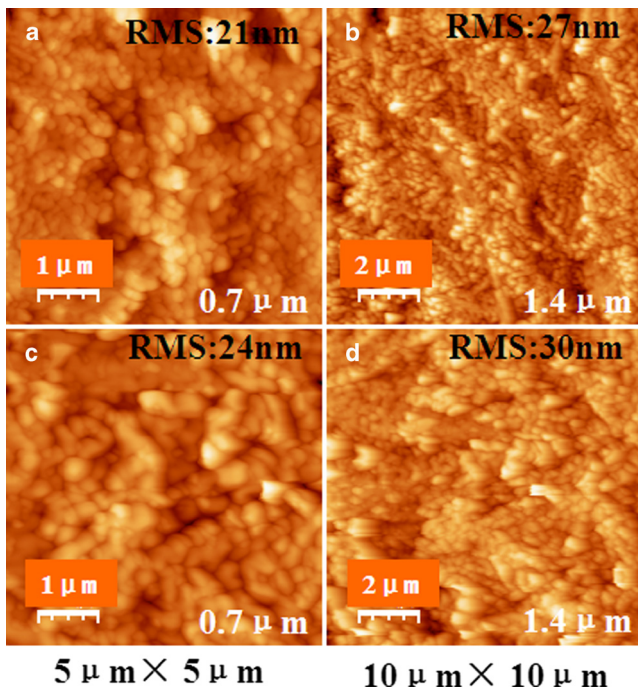


Fig. 2 AFM images of various thick films showing the typical granular structure of DyBCO/YBCO in the scale of $5 \times 5 \mu\text{m}^2$ and $10 \times 10 \mu\text{m}^2$, respectively

The XRD patterns of DyBCO/YBCO with thickness of $1.4 \mu\text{m}$, $2.1 \mu\text{m}$ and $2.8 \mu\text{m}$ are shown in Fig. 3. The scans show a pure *c*-axis oriented growth of YBCO up to a thickness of $2.8 \mu\text{m}$. Additional peaks of (110)- and (103)-oriented YBCO were observed in thicker films (in Fig. 3). The intensity of the *a*-axis peaks (YBCO(200)) increase further with thickness.

We found a little peak of BaF_2 in the sample with thickness of $2.1 \mu\text{m}$ and $2.8 \mu\text{m}$, which becomes more dominant in thicker films. The appearance of BaF_2 peaks in the thick films is typical for our MOD films. They show a common phenomenon during the chemical reaction of chemical vapor deposition (CVD); in the process of this reaction, F-Ba process is complex and the chemical reaction time is sharp; furthermore, which is intense, it is hard to avoid a small amount of BaF_2 and other impure phase (such as Ba-Cu-O) appearances.

Closed pores (marked by blue arrows in Fig. 4). Additionally, they might be a starting point for the growth of disoriented YBCO. Therefore, a reduction of the size of the particles could help to reduce the amount of pores, lower the surface and prevent disorientations.

Energy dispersive X-ray spectrometry (EDS) elemental maps of the DyBCO/YBCO multilayer film are shown in Fig. 5; elements such as Dy, Y, Ba, Cu, O, and Pt were analyzed. As seen in Fig. 5, in the middle area of DyBCO/YBCO multilayer film, almost the contact area between the second and the third layer, there are some pores,

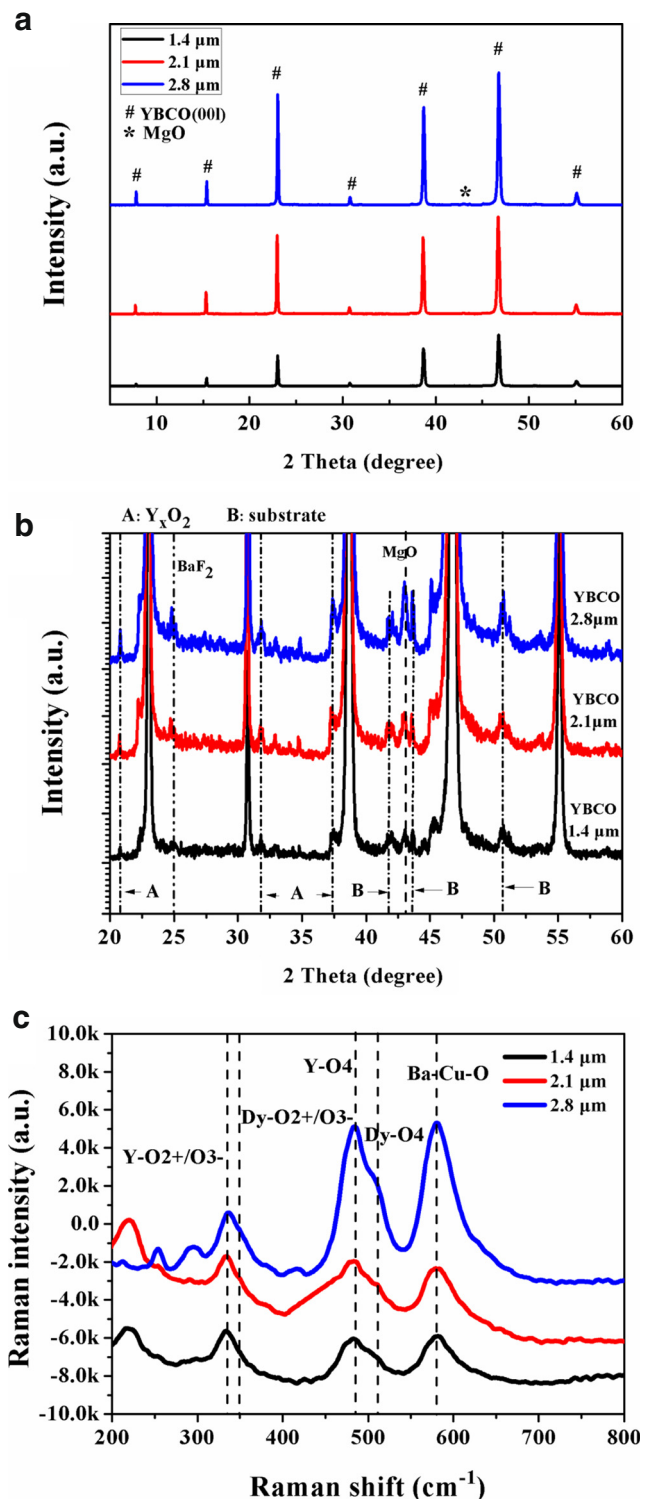
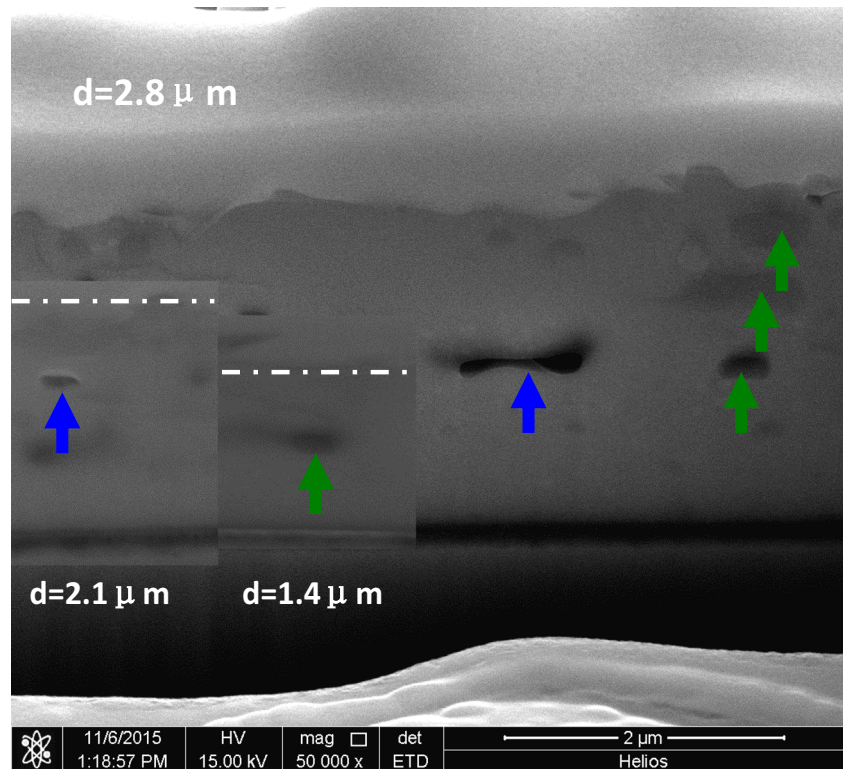


Fig. 3 XRD patterns for the samples with the thicknesses of $1.4 \mu\text{m}$, $2.1 \mu\text{m}$ and $2.8 \mu\text{m}$, respectively (a) linear vertical coordinate; (b) logarithmic vertical coordinate

which are marked with the rectangular dotted line in Fig. 5, the reason may be that during the low-temperature decomposition, Cu element diffuses faster than other elements, only left uneven distribution, and it is also possible that the

Fig. 4 FIB-SEM images of a cross section for 1.4 μm , 2.1 μm , and 2.8 μm -thick film. The inserts ($d = 1.4 \mu\text{m}$, $d = 2.1 \mu\text{m}$) are zoomed according to the scale of the 2.8 μm -thick sample. Pores (short blue arrow) and Cu-rich phase (short green arrow) can act as disorientations of YBCO

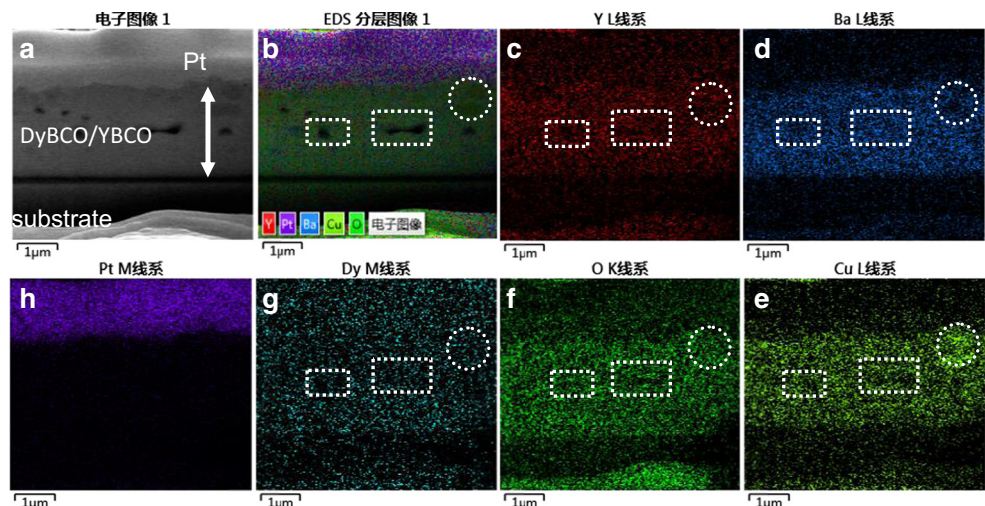


decomposition of low temperature HF gas releases excessive residual cavity. Dy, Y, and Ba elements were dispersed homogeneously in the entire film. However, Ba dispersed thickness was seen to be thinner than that with O and Cu elements which were aggregated near the film surface as oxides. These segregated precipitates can be considered as non-reacted phases which could not transform to Y123 phase, which are marked with the circular dotted line in Fig. 5.

Our measurements of the IBAD template show an in-plane FWHM value of 8.3° for LMO (111) and the typical

FWHM values of 4.0° were found for the YBCO (103) peaks. The dependence on the YBCO thickness is shown in Fig. 6a for a number of samples. We found that the peak width is slightly reduced with increasing thickness and reaches a value of around 2.06° at $d = 2.1 \mu\text{m}$. However, the peak width is rapidly increased to 2.96° when the thickness reaches 2.8 μm . The improved texture and the increasing grain size indicate some kind of growth selection mechanism, where unfavorable textured grains are overgrown. On the other hand, also, the longer processing time for thicker films may lead to an improvement of the texture

Fig. 5 Energy dispersive X-ray spectrometry (EDS) elemental maps of the DyBCO/YBCO multilayer film with thickness of 2.8 μm



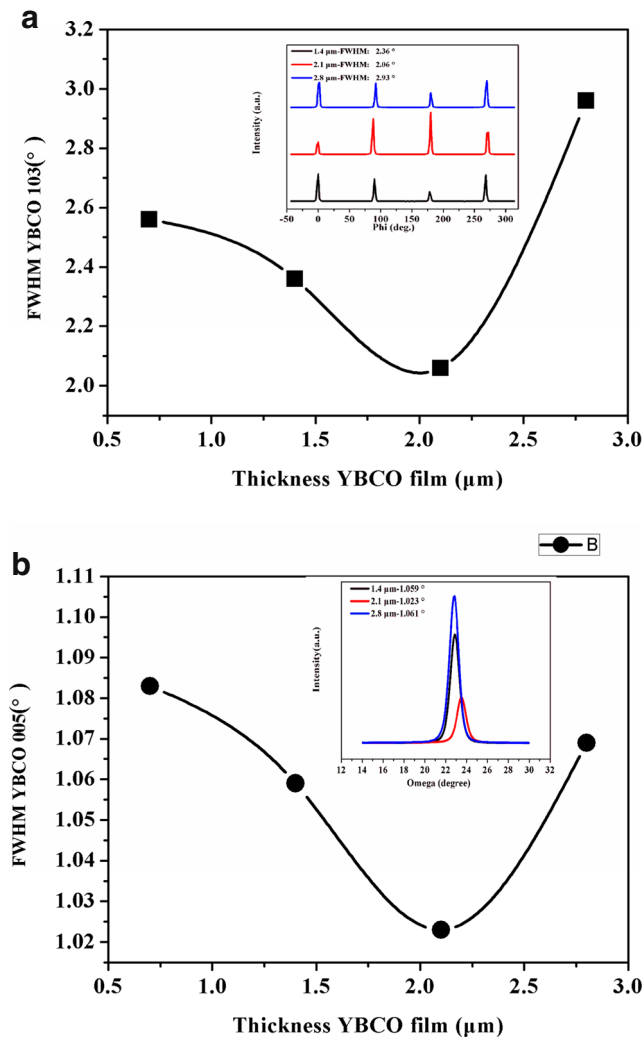


Fig. 6 In-plane FWHM of the YBCO (103) peaks **(a)** and out-plane FWHM of the YBCO (005) peaks **(b)** in dependence on the thickness of the layer. *Insert image* are in-plane and out-plane FWHM

as there is more time for the atoms to find an energetic favorable position.

In comparison, the out-of-plane alignment remained constant within the uncertainty of the measurement, with FWHM values of about 1° for YBCO (005), which is just following the same change rule of decreasing as the thickness increases from 0.7 μm to 2.1 μm, and then becomes bigger as the thickness reach to 2.8 μm.

3.2 Superconducting Properties

Figure 7a shows the inductive critical current density at 77 K under self field. In our sample, J_c reaches 3.0 MA/cm² as a maximum local value and around as the highest average value in the thinnest sample ($d = 0.7\mu\text{m}$). Clearly, the critical current density (J_c) values decreasing from 3.0 to 1.2 MA/cm² as the thickness increasing from 0.7μm

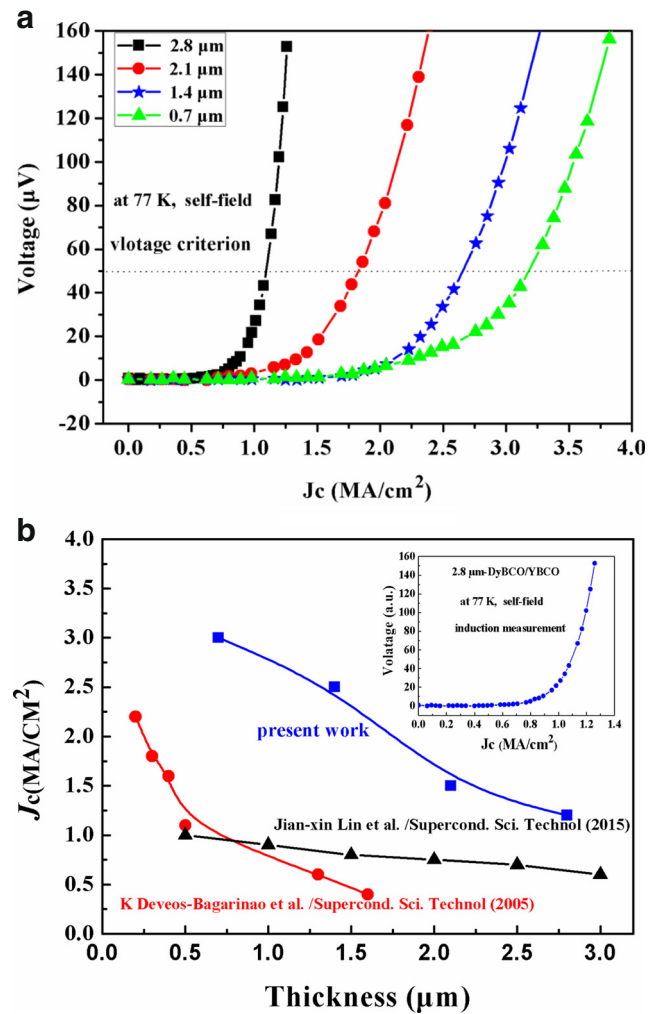


Fig. 7 Critical current density at 77 K and their thickness dependence: **a** Inductive measurement of J_c ; **b** Thickness dependence and contrast to the other published

to 2.8 μm, which dropped quickly as soon as possible (Fig. 7a). Nevertheless J_c is increasing strongly up to $d = 2.1\mu\text{m}$. Above this thickness, J_c also cannot increase as the thickness of the thick film, which may be due to the “thick effect” that was observed in [16, 17]. This limitation is in line with the appearance of disoriented YBCO grains and large impure phase, as described above. Additionally, the increasing volume fraction of pores and Cu-rich phase are limiting the superconducting cross section and J_c .

4 Conclusions

In summary, we deposited DyBCO/YBCO multilayer thick films with a thickness ranging from 0.7 μm to 2.8 μm on IBAD-MgO substrate buffered by LMO substrate. We observed the RMS of the thick surface becoming coarsened

with an increasing of the thickness, as well as the appearance of disorienting and impure phases for films thicker than $2.1 \mu\text{m}$. In-plane and out-plane texture decreases as the thickness increasing, when the thickness reach a certain thickness ($d = 2.1 \mu\text{m}$) which will become bigger than before. The YBCO film seems to be compressed in-plane up to $d = 2.1 \mu\text{m}$ leading to an increased c -axis lattice parameter and higher T_c in thinner films. At 77 K, a J_c of around 3.0 MA/cm^2 was measured in the thinnest sample ($d = 0.7 \mu\text{m}$). As the film thickness increases to $2.8 \mu\text{m}$, J_c drops to a value of 1.2 MA/cm^2 . We conclude that LMO buffered IBAD-MgO can act as a sufficient template for YBCO-coated conductors.

Acknowledgments This work was supported in part by Shanghai Key Laboratory of High Temperature Superconductors (14DZ2260700), the Science and Technology Commission of Shanghai Municipality (13111102300 and 14521102800), the National Natural Science Foundation of China (51572165, 11174193 and 51202141).

References

- Iguchi, T., Araki, T., Yamada, Y., Hirabayashi, I., Ikuta, H.: *Supercond. Sci. Technol.* **15**, 1415–1420 (2002)
- Rupich, M.W., Verebelyi, D.R., Zhang, W., Kodenkandath, T., Li, X.: *Mater. Res. Soc. Bull.* **29**, 572–578 (2004)
- Miyata, S., Matsuse, K., Ibi, A., Izumi, T., Shiohara, Y., Goto, T.: **26**, 045020 (2013)
- Wen, H.H., Yang, W.L., Zhao, Z.X.: *Physica C* **341**, 1735–1738 (2000)
- Engel, S., Thersleff, T., Hühne, R., Schultz, L., Holzapfel, B.: *Appl. Phys. Lett.* **90**, 102505 (2007)
- MacManus-Driscoll, J.L., Foltyn, S.R., Maiorov, B., Jia, Q.X., Wang, H., Serquis, A., Civale, L., Lin, Y., Hawley, M.E., Maley, M.P., Peterson, D.E.: *Appl. Phys. Lett.* **86**, 032505 (2005)
- Cai, C., Holzapfel, B., Hänisch, J., Fernandez, L., Schulz, L.: *Appl. Phys. Lett.* **84**, 377 (2004)
- Obradors, X., Martínez-Julián, F., Zalamova, K., Vlad, V.R., Pomar, A., Palau, A., Llordés, A., Chen, H., Coll, M., Ricart, S., Mestres, N., Granados, X., Puig, T., Rikel, M.: *Physica C* **482**, 58–67 (2012)
- Matsui, H., Sohma, M., Yamaguchi, I., Manabe, T., Kumagai, T.: *Physics Procedia* **36**, 1643–1648 (2012)
- Jian, H., Shao, D., Yang, Z., Zhu, X., Sun, Y.: *Physica C* **488**, 39–45 (2013)
- Miura, M., Kato, T., Yoshizumi, M., Yamada, Y., Izumi, T., Hirayama, T., Shiohara, Y.: *Appl. Phys. Express* **2**, 023002 (2009)
- Obradors, X., Puig, T.: *Supercond. Sci. Technol.* **27**, 4 (2014)
- Fang, J., Wu, N., Tong, W., Ling, L., Zhang, L., Xi, C., Pi, L., Sun, Y., Zhan, Y.: *J. Appl. Phys.* **113**, 083904 (2013)
- Nakamura, T., Nakahata, K., Yoshizumi, M., Izumi, T., Shiohara, Y., Kimura, K., Hasegawa, T., Kato, T., Hirayama, T.: *Physics Procedia* **45**, 153–158 (2013)
- Araki, T., Hirabayashi, I.: *Supercond. Sci. Technol.* **16**, 71–94 (2003)
- Develos-Bagarinao, K., Yamasaki, H., Nie, J.C., Nakagawa, Y.: *Supercond. Sci. Technol.* **18**, 667–674 (2005)
- Foltyn, S.R. et al.: *Appl. Phys. Lett.* **75**, 3692 (1999)